Widnall instabilities in vortex pairs

Denis Sipp and Laurent Jacquin
ONERA, 8 rue des Vertugadins, 92190 Meudon, France

(Received 28 November 2001; accepted 26 March 2003; published 5 June 2003)

In this article we analyze the cooperative three-dimensional short-wave instabilities developing on concentrated vortex dipoles that have been obtained by means of two-dimensional direct numerical simulations. These dipoles are characterized by their aspect ratio a/b where a is the radius of the vortices based on the polar moments of vorticity and b is the separation between the vortex centroids. In the inviscid case, we show that the selection of the antisymmetric eigenmode smoothly increases with a/b: for $a/b=0.208$, the amplification rate of the antisymmetric eigenmode is only 1.4% larger than the amplification rate of the symmetric eigenmode. When $a/b=0.288$, this difference increases up to 7%. The results of the normal mode analysis may be compared to those of an asymptotic stability analysis of a Lamb–Oseen vortex subjected to a weak straining field, following Moore and Saffman [Proc. R. Soc. London, Ser. A **346**, 413 (1975)]. This theory shows that the instability may occur whenever two Kelvin waves exist with the same frequency ω, the same axial wavenumber k and with azimuthal wavenumbers m and $m+2$. Contrary to the case of a Rankine vortex [Tsai and Widnall, J. Fluid Mech. **73**, 721 (1976)], the presence of critical layers in a Lamb–Oseen vortex prevents a large number of possible resonances. For example, resonances between $m=-2$ and $m=0$ modes lead to damped modes. The only resonances that occur are related to the stationary ($\omega=0$) bending waves ($m=\pm 1$) obtained for specific values of the axial wavenumber. All these predictions are found to be in good agreement with the results obtained by the stability analysis of the considered vortex pairs. At last, we present a nonautonomous amplitude equation which takes into account all effects of viscosity, i.e., the viscous damping of the amplification rate of the perturbation but also the increase of the dipole aspect ratio a/b due to the viscous diffusion of the basic flowfield. The low-Reynolds number experiment of Leweke and Williamson [J. Fluid Mech. **360**, 85 (1998)] is revisited under the light of these theoretical results. We show that these theoretical results yield predictions for the amplification rate and for the wavenumber that agree with the experimental observations.
[DOI: 10.1063/1.1575752]

I. INTRODUCTION

In this article, we analyze three-dimensional linear instabilities of the family of concentrated two-dimensional vortex dipoles given in Ref. 1. These dipoles are parametrized by their dipole aspect ratio a/b where a is the radius of the vortices based on the polar moments of vorticity and b is the separation between the vortex centroids.

The results presented in this paper may be helpful to explain some of the features obtained in the Leweke and Williamson experiment.[2] Here, we focus on the short-wave perturbation leaving aside the long-wave instability.[3] These authors observed the selection and the growth of a short-wave antisymmetric eigenmode characterized by the nondimensional wavenumber $kb=8.16$ and the nondimensional amplification rate $\sigma 2\pi b^2/\Gamma=0.94$ where Γ stands for the circulation magnitude of each vortex. One of the objectives of the present paper is to give theoretical support to these observations.

The short-wave instability has been fully described in the inviscid case by Moore and Saffman[4] for a weakly stretched vortex. Using a multiple time scale analysis based on the small parameter a^2/b^2, these authors showed that instability may arise through a resonance of the straining field with two Kelvin waves of the same axial wavenumber k, of the same frequency ω and with the azimuthal wavenumbers m and $m+2$. Tsai and Widnall[5] showed, in the case of a Rankine vortex, that several resonances of this kind occur. This happens, for instance, for Kelvin waves with $(m=-1,m+1=1)$ but also when $(m=-2,m+2=0)$ or $(m=1,m+2=3)$. For a vortex with a smooth vorticity distribution like the Lamb–Oseen vortex, one has to account for the existence of critical layers where the azimuthal speed of the wave equals the angular rotation of the axisymmetric vortex. Widnall, Bliss and Tsai[6] apparently overlooked these aspects since they concluded that the case of smooth vorticity distributions is qualitatively equivalent to the case of a Rankine vortex. In the present article we aim at showing the differences between a Lamb–Oseen and a Rankine vortex in terms of inertial waves and short-wave perturbations. We also aim at understanding if this simplified model, i.e., a weakly stretched Lamb–Oseen vortex, is able to capture the essential physics of the development of a short-wave perturbation in a complex flowfield like a vortex pair.

The effect of viscosity has been analyzed in the case of a short-wave perturbation developing on a homogeneous elliptical flow. Landman and Saffman[7] gave a correction term for the amplification rate taking into account the viscous damping effect on the perturbation. Note that the basic flowfield is not affected by viscosity in this case since velocity gradients in homogeneous flows are constant. In the present article we thoroughly analyze the effects of viscosity in the case of a short-wave perturbation developing on vortex dipoles. We recall that viscosity affects both the basic flowfield through the increase of the aspect ratio a/b and the perturbation through the modification of the amplification rate.

The selection of the antisymmetric eigenmode as observed in the Leweke and Williamson experiment escapes to the asymptotic method used by Moore and Saffman[4] since the theory only accounts for the dynamics of one vortex, the other being simply modeled by the presence of the straining field. Note that Leweke and Williamson[2] showed on the basis of a qualitative argument that the antisymmetric eigenmode should be favored. But a quantitative result still lacks to sustain their argument. Hence, one of the objectives of this paper is to achieve a normal mode analysis of vortex dipoles that are characteristic of the Leweke and Williamson experiment in order to investigate the properties of the symmetric and antisymmetric eigenmodes. Billant, Brancher and Chomaz[8] achieved that work in the case of the Lamb–Chaplygin dipole.[8–10] Their results confirmed that the antisymmetric mode is promoted but their basic flowfield is characterized[1] by an aspect ratio $a/b=0.4478$ much thicker than that obtained in the experiment where $a/b\sim0.25$.

Note also that the weakly nonlinear regime of the Widnall instability has been described in Ref. 11. It was shown that these instabilities saturate, as observed in the experiment of Leweke and Williamson.

The present paper is organized as follows. In Sec. II, we present the dipole family obtained in Ref. 1. In Sec. III, we analyze the inviscid stability of two vortex pairs of the dipole family, which are characterized by aspect ratios a/b equal to 0.208 and 0.288. In Sec. IV, we focus on the inviscid stability of a stretched Lamb–Oseen vortex. We show that this simplified model explains well the results obtained in Sec. III. Section V is dedicated to the influence of viscosity. We will present a nonautonomous amplitude equation taking into account both the effect of viscosity on the basic flow and on the perturbation. We will show that these predictions are fully compatible with the experimental observations of Leweke and Williamson.

II. PRESENTATION OF THE BASIC FLOWFIELD

In Ref. 1, it was shown using 2-D direct numerical simulations that various initial dipolar vorticity distributions evolve towards a specific family of dipoles parametrized by the dipole aspect ratio a/b. This convergence was achieved through viscous effects. Nevertheless, viscosity is sufficiently small so that we can consider these solutions as steady on the time scales considered here. The vorticity distributions of two vortex pairs belonging to this dipole family and characterized by $a/b=0.208$ and $a/b=0.288$ are shown in Fig. 1.

We first show that these basic flows exhibit weakly stretched Lamb–Oseen type vortices. Figure 2 represents, versus a/b, the levels of vorticity $W_L 2\pi a^2/\Gamma$ and strain $\epsilon_L 2\pi b^2/\Gamma$ obtained in the center of the vortices in two direct numerical simulations presented in Ref. 1 and labeled (α) and (β). In both simulations, the initial flowfield consists of two counter-rotating Lamb–Oseen vortices and the Reynolds number is given by $\mathrm{Re}=\Gamma/\nu=3142$. At $t=0$, the aspect ratio a/b of the dipoles is equal to 0.067 in simulation (α) and 0.134 in simulation (β). The strain $\epsilon_L 2\pi b^2/\Gamma$ is equal to 1 at $t=0$ in both simulations due to the choice of the initial flowfields. Since the initial flowfields are not steady solutions of the Euler equations, the flowfields quickly evolve on the advective time scale $T_a=2\pi a^2/\Gamma$. This can be observed in Fig. 2 with the large oscillations of the strain $\epsilon_L 2\pi b^2/\Gamma$ as a function of a/b. The dipole then rapidly adapts to a quasi-steady solution of the Euler equations where the strain $\epsilon_L 2\pi b^2/\Gamma$ and the vorticity $W_L 2\pi a^2/\Gamma$ are close to 2.5 and 2, respectively. Following Eloy and Le Dizès,[12] these values are characteristic of weakly stretched Lamb–Oseen vortices.

Second, we show that the flowfield obtained in the experiment of Leweke and Williamson[2] is very close to the vortex pairs which belong to the family of vortex dipoles presented in Ref. 1. It was shown in Ref. 1 that various initial

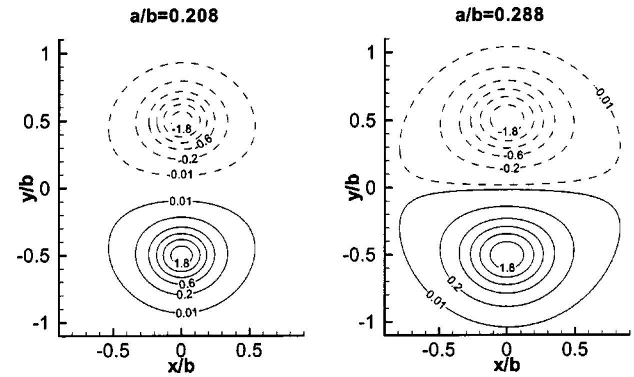

FIG. 1. Vorticity distributions of the dipoles for $a/b=0.208,0.288$. The isolevels represent the vorticity $W 2\pi a^2/\Gamma$. Dashed lines represent negative values. These dipoles are steady solutions of the Euler equations (see Ref. 1).

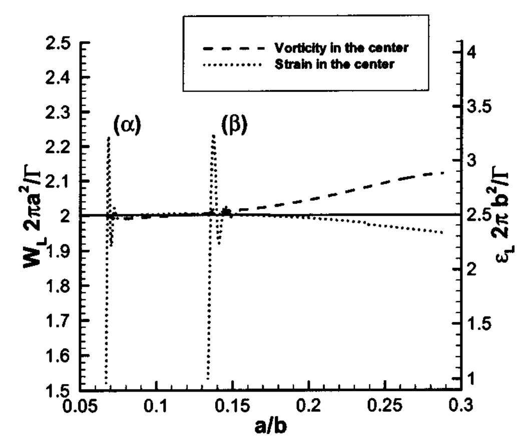

FIG. 2. Vorticity and strain in the center of the vortices versus a/b in the direct numerical simulations. W_L and ϵ_L characterize, respectively, the strength of the symmetric and the antisymmetric part of the velocity gradient tensor in the center of the vortices.

dipolar vorticity distributions evolve through viscous diffusion towards a specific family of dipoles parametrized by a/b. In particular, Fig. 5 in this article shows that all vorticity distributions characterized by $a/b=0.134$ at the beginning of the simulation converged towards this family (for Re=3142 and Re=15708) when the dipole aspect ratio reached $a/b=0.20$. Now, Leweke and Williamson showed that shortly after the stopping of the plate motion the velocity profile of the flowfield can be fitted by the superposition of two counter-rotating Lamb–Oseen vortices with $a/b=0.15$. The Reynolds number of the experiment being quite small ($\mathrm{Re}=\Gamma/\nu=2750$), this aspect ratio then progressively increases due to the viscous diffusion of the basic flowfield. For instance, the instability starts to be visible when $a/b=0.24$ and the linear regime holds on at least until $a/b=0.285$. Hence, it seems obvious that the experimental 2-D dipole structures remain very close to the structures of the dipole family vortex pairs presented in Ref. 1.

III. INVISCID STABILITY ANALYSIS OF THE VORTEX PAIRS

Linearizing the Navier–Stokes equations around the steady basic flow, we look for unstable normal modes. For the basic flow lying in the (x,y) plane, the normal modes are sought under the form $e^{\sigma t}e^{ikz}\phi(x,y)$, where $\phi=u',v',w',p'$ stands for the velocity and pressure perturbations. k is the real Oz wavenumber and σ is the complex amplification rate. The vorticity field being skew-symmetric with respect to $y=0$, the eigenmodes can be decomposed into two independent subsets:

(1) the antisymmetric modes where u' is odd and v' is even with respect to $y=0$;
(2) the symmetric modes where u' is even and v' is odd with respect to $y=0$.

The numerical procedure used to obtain these normal modes is based on a matrix eigenvalue method. A spectral Chebyshev–Gauss collocation method is used to discretize the (x,y) derivatives. More details are given in Appendix A.

We first achieve inviscid stability analyses leaving aside the influence of the Reynolds number which will be thoroughly investigated in Sec. V.

The results of the inviscid stability analyses ($\mathrm{Re}=\Gamma/\nu=\infty$) are given in Fig. 3 for $a/b=0.208$ and in Fig. 4 for $a/b=0.288$. Each plot gives the amplification rate $\sigma 2\pi b^2/\Gamma$ of the symmetric (filled triangles) and antisymmetric (empty circles) unstable eigenmodes versus ka. All unstable eigenmodes are nonoscillating (the imaginary part of σ is zero).

In the case $a/b=0.208$, we obtain several distinct unstable ka intervals where the symmetric and antisymmetric amplification rates are very close. For example, for $ka=2.26$, the amplification rate of the antisymmetric eigenmode is 1.4% larger than the amplification rate of the symmetric eigenmode. This shows that the Widnall instabilities may develop independently on each vortex and that there is almost no linear selection of the antisymmetric mode. The results of the case $a/b=0.288$ show that the amplification

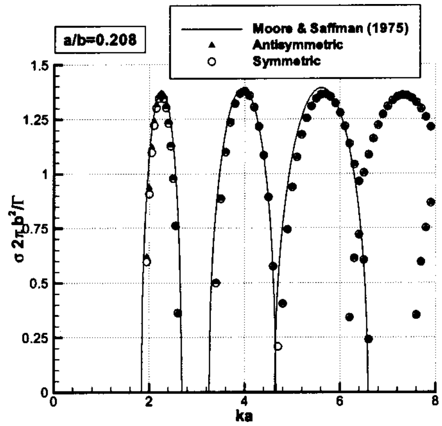

FIG. 3. Widnall instabilities for the dipole characterized by $a/b=0.208$ and $\mathrm{Re}=+\infty$.

rates of the antisymmetric modes for $1.2\leqslant ka\leqslant 3.2$ are approximately 7% larger than those of the symmetric modes. In the case of a Lamb–Chaplygin dipole, characterized by $a/b=0.4478$, Billant *et al.*[8] found that the amplification rates of the corresponding antisymmetric eigenmodes were approximately 18% larger than those of the symmetric modes. Thus, the selection process of the antisymmetric instabilities smoothly increases with a/b. One gets: +1.4% when $a/b=0.208$, +7% when $a/b=0.288$ and +18% when $a/b=0.4478$.

In Fig. 5, we give the Oz vorticity of the antisymmetric unstable eigenmode corresponding to $a/b=0.208$ and $ka=2.26$. It represents a symmetric plot with respect to $y=0$ (an antisymmetric mode is characterized by a symmetric plot for the vertical vorticity) and is compound of dipoles, characteristic of the elliptic instabilities found in Refs. 13–15.

IV. STABILITY ANALYSIS OF A STRETCHED LAMB–OSEEN VORTEX

Moore and Saffman explained[4] how a vortex column in a weak straining field could be destabilized. The stability analysis of the Rankine vortex in a weak straining field has been given by Tsai and Widnall.[5] Here, we show that contrary to what was argued by Widnall *et al.*,[6] a Lamb–Oseen vortex is quite different from a Rankine vortex as far as the

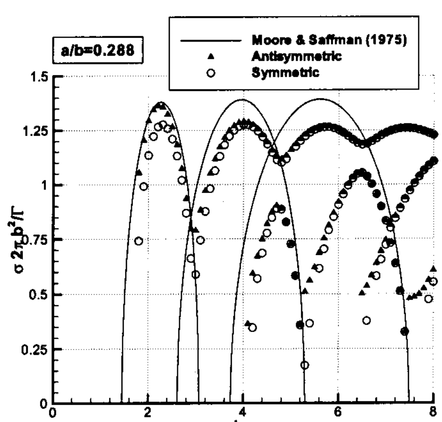

FIG. 4. Widnall instabilities for the dipole characterized by $a/b=0.288$ and $\mathrm{Re}=+\infty$.

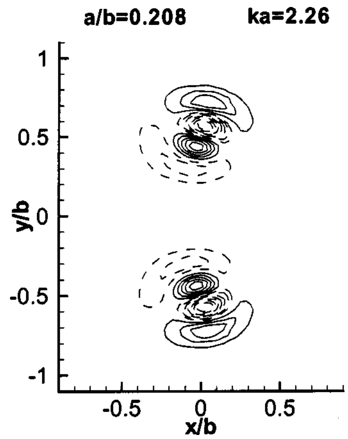

FIG. 5. Vertical vorticity of antisymmetric unstable eigenmode for $a/b = 0.208$, Re$=+\infty$ and $ka=2.26$. Dashed lines represent negative values.

Widnall instabilities are concerned. Note that some partial results have been given for the Lamb–Oseen vortex by Eloy and Le Dizès.[12]

We consider a Lamb–Oseen vortex of circulation Γ and radius a in a weak straining field of strength $\epsilon=\Gamma/2\pi b^2$. The angular rotation $\Omega(r)$ of the Lamb–Oseen vortex reads as

$$\Omega(r)=\frac{\Gamma}{2\pi r^2}[1-e^{-r^2/a^2}]. \tag{1}$$

The strain is characterized by the streamfunction $\psi=-1/2\epsilon f(r)\cos 2\theta$. As shown by Moore and Saffman,[4] the radial structure of the function $f(r)$ is determined so as to obtain a steady flow on the $O(1/\epsilon)$ time scale. One obtains

$$f''+\frac{f'}{r}-\left(\frac{3\Omega'+r\Omega''}{r\Omega}+\frac{4}{r^2}\right)f=0, \tag{2}$$

with the following normalization condition: $f(r)/r^2\rightarrow 1$ as $r\rightarrow\infty$. A representation of the function $f(r)/r^2$ has been given in Fig. 1 of Ref. 12. The straining field is 2.5 times stronger in the center of the Lamb–Oseen vortex than at infinity. As mentioned in Sec. II, this value has been retrieved (see Fig. 2) in the direct numerical simulations performed in Ref. 1, showing that the dipole family exhibits vortices that are close to the theoretical model presented in this section.

A. The Widnall instability mechanism

We consider a flowfield constituted of the axisymmetric Lamb–Oseen vortex, the above defined straining field of strength ϵ and a small perturbation. We substitute this development in the incompressible Euler equations and linearize into the disturbance field. We then perform a multiple time scale analysis based on the time scales $2\pi a^2/\Gamma$ and $1/\epsilon$ (we suppose that $2\pi a^2/\Gamma \ll 1/\epsilon$).

(1) On the time scale $2\pi a^2/\Gamma$, we obtain a linear oscillator which selects the Kelvin waves. The numerical procedure to obtain these Kelvin waves is given in Sec. IV B. We now suppose that there exists two Kelvin waves A and B with the same nondimensional frequency $(\omega 2\pi a^2/\Gamma)_c$, the same nondimensional axial wavenumber $(ka)_c$ and with azimuthal wavenumbers m and $m+2$. The perturbation is then chosen as a particular linear combination of the two spatial (r,θ) structures of the Kelvin waves A and B. The axial wavenumber ka of this perturbation is chosen to be close to $(ka)_c$:

$$\frac{\Gamma}{2\pi a^2\epsilon}[ka-(ka)_c]=O(1). \tag{3}$$

(2) On the time scale $1/\epsilon$, we obtain the same linear oscillator as before with a forcing term on the right hand side (rhs). Removing the resonant part of this forcing term yields the following equation for the complex amplification rate σ of the perturbation:

$$\left[\frac{\sigma}{\epsilon}+i\alpha_A\frac{\Gamma}{2\pi a^2\epsilon}[ka-(ka)_c]\right] \times\left[\frac{\sigma}{\epsilon}-i\alpha_B\frac{\Gamma}{2\pi a^2\epsilon}[ka-(ka)_c]\right]=\beta_A\beta_B, \tag{4}$$

where α_A, β_A, α_B and β_B are complex constants that can be computed numerically.

If the resulting real part of σ is positive, then the flow is unstable. In the general case $[(\omega 2\pi a^2/\Gamma)_c,(ka)_c,m]$, one has to evaluate numerically all the constants to determine σ.

In the particular case $(m=-1, m+2=1)$, there exists stationary $(\omega 2\pi a^2/\Gamma)_c=0$ Kelvin waves for fixed values of $(ka)_c$. Here, due to the symmetries of the basic flow, one can show that: $\alpha_A=\alpha_B=\alpha$ and $\beta_A=\beta_B=\beta$ are real numbers. Thus

$$\frac{\sigma}{\epsilon}=\beta\sqrt{1-\left(\frac{\alpha}{\beta}\frac{\Gamma}{2\pi a^2\epsilon}[ka-(ka)_c]\right)^2}. \tag{5}$$

A narrow band of instability exists. Its width is $|ka-(ka)_c|<\beta/\alpha 2\pi a^2\epsilon/\Gamma$ and the peak of instability is reached for $ka=(ka)_c$ (in which case $\sigma=\epsilon\beta$).

B. Kelvin waves of a Lamb–Oseen vortex

In this section, we study the Kelvin waves on the Lamb–Oseen vortex, in order to determine the values of (ω,m,k) where there exists two Kelvin waves of the same frequency ω, of the same axial wavenumber k and with azimuthal wavenumbers m and $m+2$.

We use a shooting method to solve the eigenvalue problem of a Lamb–Oseen vortex for $m=0$, $m=\pm 1$ and $m=\pm 2$ Kelvin waves.

1. Method

We linearize the incompressible Euler equations around the Lamb–Oseen vortex and introduce the following small perturbations:

$$(v_r',v_\theta',v_z',p')=(iF(r),G(r),H(r),P(r))e^{i(kz+m\theta+\omega t)}, \tag{6}$$

where v_r', v_θ' and v_z', are the radial, azimuthal and axial components of the velocity and p' is the pressure.

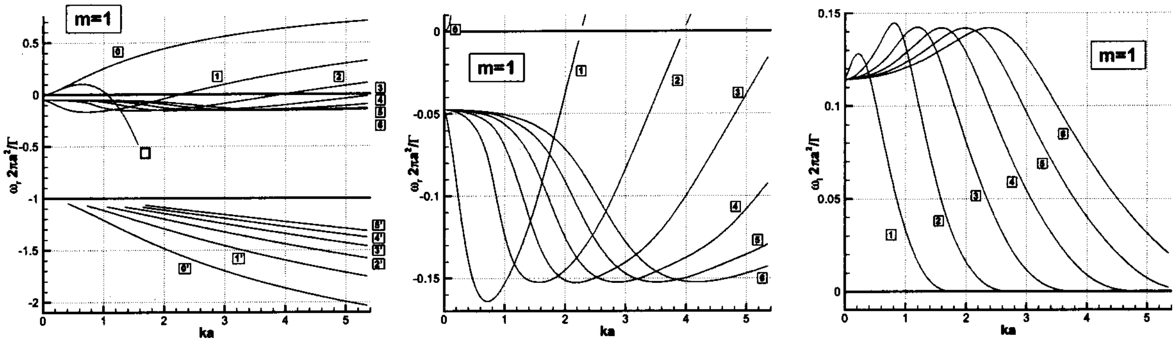

FIG. 6. Resonances with $m=\pm 1$ modes. Left: frequencies $\omega_r 2\pi a^2/\Gamma$ vs ka. Center: frequencies $\omega_r 2\pi a^2/\Gamma$ in the critical layer zone versus ka. Right: damping rates $\omega_i 2\pi a^2/\Gamma$ versus the wavenumber ka. The solid line labeled with an empty square represents formula (10).

Following Refs. 16 and 17 we are led to the following second order equation:

$$Z''+\left(\frac{1}{r}+\frac{2\gamma'}{\gamma}-\frac{2k^2r}{m^2+k^2r^2}\right)Z'-\left(k^2+\frac{m^2}{r^2}+\frac{2m\Omega'}{\gamma r}-\frac{4mk^2\Omega}{\gamma(m^2+k^2r^2)}-\frac{2k^2\Omega}{\gamma^2 r}(r^2\Omega)'\right)Z=0, \tag{7}$$

where a prime denotes the operator d/dr and

$$Z(r)=\frac{rF(r)}{\gamma(r)}, \tag{8}$$

$$\gamma(r)=\omega+m\Omega(r). \tag{9}$$

This equation along with the boundary conditions $Z(0)=Z(\infty)=0$ constitutes an eigenvalue problem for ω.

The solutions are obtained by the following procedure.

(1) We transform the second order differential equation of $Z(r)$ (7) into a first order differential equation of $(Z(r),Z'(r))$.
(2) We consider the asymptotic behavior for $(Z(r),Z'(r))$ at $r=0$ and $r=\infty$.
(3) Starting from these asymptotic values, the solution of (7) is obtained at a given radius r_f. This leads to two couples: $(Z_+(r_f),Z'_+(r_f))$ and $(Z_-(r_f),Z'_-(r_f))$. Typically, we start with $r/a=0.1$ and $r/a=20$. Integration is achieved with a classical fourth order Runge–Kutta scheme.
(4) We search values of ω such as the Wronskian $Z_+(r_f)Z'_-(r_f)-Z_-(r_f)Z'_+(r_f)$ is zero. The iterative scheme is performed via a Newton–Raphson method in the complex ω plane. A guess value is therefore needed to start this process.
(5) At the critical points $\gamma(r_c)=0$, the integration path is modified according to the criterion given in Ref. 18.

2. Resonances with $m=\pm 1$ modes

The oscillation frequencies of the modes $m=\pm 1$ are given in the left plot of Fig. 6. We compare these results with those obtained for the Rankine vortex (see Ref. 19, Fig. 12.1-4, p. 233). Eigenfunctions corresponding to various modes are identified, as in the Sturm–Liouville theory, by the number of their zeros n in the radial direction (the primary mode, labeled $n=0$ has no zeros, the mode labeled $n=1$ has one zero, etc.).

The results are similar to those of a Rankine vortex when $\omega_r 2\pi a^2/\Gamma>0$ or $\omega_r 2\pi a^2/\Gamma<-1$, i.e., when no critical layers are present. In this case, the modes are purely oscillatory, i.e. $\omega_i=0$. The asymptotic behavior, for $ka\to 0$, of the branch labeled 0, was given in Refs. 20 and 21:

$$\omega\frac{2\pi a^2}{\Gamma}=\frac{(ka)^2}{2}\left(\ln\frac{1}{ka}+\frac{\ln 2-\gamma}{2}\right), \tag{10}$$

where $\gamma=0.577215$ is Euler's constant. This branch is called the slow branch since both the frequency ω and the phase speed $c=\omega/k$ tend towards zero as the wavenumber k goes to zero. On the other hand, the branches labeled $0'$, $1'$, $2'$, etc., are called fast branches because $c=\omega/k\to\infty$ as $k\to 0$ [see formula (56a) in Ref. 21]. We can see that resonances may occur for specific values of the nondimensional wavenumber ka where $\omega=0$.

Now, the linear dynamics of the Lamb–Oseen vortex completely differs from that of the Rankine vortex when $-1<\omega_r 2\pi a^2/\Gamma<0$, i.e., when critical layers are present. In the central and right plots of Fig. 6, we have sketched $\omega_r 2\pi a^2/\Gamma$ and $\omega_i 2\pi a^2/\Gamma$ against the vertical wavenumber ka in this region. We see that the modes are no longer purely oscillatory but are damped. This is due to the presence of critical layers in the eigenmode. In critical layers, the azimuthal speed of the wave equals the angular rotation of the axisymmetric vortex. Regularization of the critical layer is achieved by viscosity thanks to the criterion given by Lin.[18] Shortly speaking, this criterion states that the inviscid case should be an asymptotic limit of the viscous case when viscosity tends to zero. More details are given in Appendix B.

The main consequence here is that, contrary to the case of the Rankine vortex, there is no resonance between the $n=0$ branch and the $n=1,2,...$ branches. The conclusion is that the only possible resonances are those which occur at $\omega=0$, i.e., $(\omega=0,m=\pm 1,ka=2.26)$, $(\omega=0,m=\pm 1,ka=3.96)$, $(\omega=0,m=\pm 1,ka=5.61)$, etc.

Note that critical layers may also be regularized thanks to nonlinearities.[22–24] In this case, the Kelvin waves in the critical layer zone could be purely oscillatory again. Actually, the nature of the critical layer (viscous or nonlinear) depends

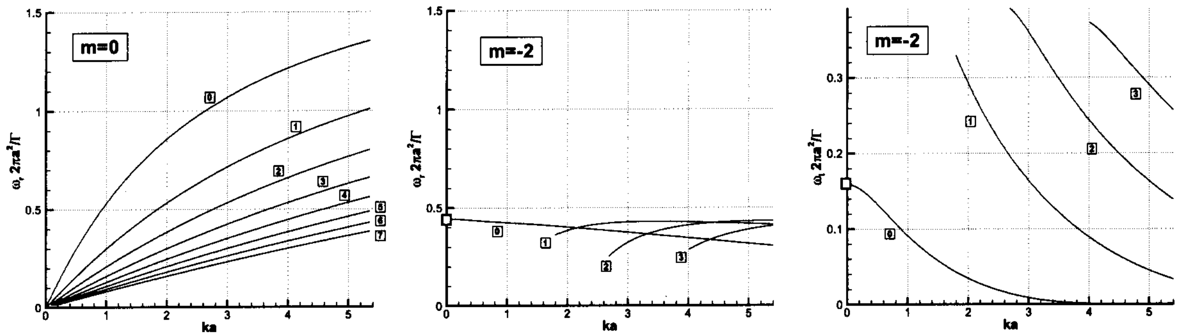

FIG. 7. Resonances with $m=0$ and $m=2$ modes. Left: frequencies $\omega_r 2\pi a^2/\Gamma$ of $m=0$ modes versus ka. Center: frequencies $\omega_r 2\pi a^2/\Gamma$ of $m=-2$ modes in the critical layer zone versus ka. Right: damping rates $\omega_i 2\pi a^2/\Gamma$ of $m=-2$ modes versus ka. The empty squares represent the values obtained by Le Dizès (Ref. 24) in the two-dimensional case.

on a parameter (the so-called Haberman parameter in the two-dimensional case), which compares the effect of viscosity to the effect of nonlinearities (the amplitude of the Kelvin waves) in the critical layer.

3. Resonances between $m=0$ and $m=-2$ modes

The oscillation frequencies of the modes $m=0$ are given in the left plot of Fig. 7. A comparison with the case of a Rankine vortex given in Ref. 19, Fig. 12.1-2, p. 231, shows that the dynamics of the two vortex models are similar. This is due to the fact that there is no critical layer in the case $m=0$.

The case $m=-2$ is similar to the case $m=1$. The critical layer zone corresponds now to the region $0<\omega_r 2\pi a^2/\Gamma<2$. As seen in the central and right plots of Fig. 7 where we have represented the first four co-rotating Kelvin waves, the modes become quickly damped as ka decreases. Hence, a resonance with the $m=0$ modes leads to damped modes. This is different from the case of the Rankine vortex,[5] for which resonances with $m=0$ and $m=-2$ Kelvin waves exist.

C. Stability analysis of a stretched Lamb–Oseen vortex

In this section, we consider the values of (ω,m,k) where there exists two Kelvin waves of the same frequency ω, of the same axial wavenumber k and with azimuthal wavenumbers m and $m+2$. These values have been determined in the previous section. Indeed, we have shown that the only possible resonances are the following: $[\omega=0,m=\pm 1,(ka)_c=2.26]$, $[\omega=0,m=\pm 1,(ka)_c=3.96]$ and $[\omega=0,m=\pm 1,(ka)_c=5.61]$, etc. In each case, we apply the multiple time scale analysis presented in Sec. IV A and determine the amplification rate σ. Since $\epsilon=\Gamma/2\pi b^2$, the unstable amplification rate reads as

$$\sigma 2\pi b^2/\Gamma=\beta\sqrt{1-([ka-(ka)_c]\alpha/\beta b^2/a^2)^2}, \qquad (11)$$

where α and β are real constants. A narrow band of instability exists. Its width is $|ka-(ka)_c|<\beta/\alpha a^2/b^2$ and the peak of instability is reached for $ka=(ka)_c$ in which case $\sigma 2\pi b^2/\Gamma=\beta$.

We have the following numerical results for the bending wave labeled 1. Maximum instability occurs for $(ka)_c=2.26$ with an amplification rate equal to $\sigma 2\pi b^2/\Gamma=1.38$. The width of the unstable band is $|ka-(ka)_c|<8.68a^2/b^2$. For the bending waves labeled 2 and 3, the unstable bands are centered at $(ka)_c=3.96$ and $(ka)_c=5.61$, respectively, the corresponding maximum amplification rates $\sigma 2\pi b^2/\Gamma$ being 1.39 in both cases. The width of the unstable bands $|ka-(ka)_c|$ are $14.4a^2/b^2$ and $20.1a^2/b^2$, respectively. The same results were found by Eloy and le Dizès.[12]

D. Comparison between the stability analyses of the vortex pairs and the stretched Lamb–Oseen vortex

The solid lines in Figs. 3 and 4 represent the results of the asymptotic stability analysis. In the case $a/b=0.208$, we see that the symmetric and antisymmetric amplification rates collapse on the three curves given by the asymptotic stability analysis. Note also that no resonances between $m=0$ and $m=-2$ modes have been found in the normal mode analyses. This is in accordance with the conclusions of Sec. IV B. This is different from the case of the Lamb–Chaplygin dipole,[8] which exhibits an unstable band corresponding to this resonance.

V. EFFECT OF VISCOSITY

A. Introduction

The dipole aspect ratio in the experiment of Leweke and Williamson[2] is found to be equal to $a/b=0.15$ just after the stopping of the plate motion at $t\Gamma/(2\pi b^2)=1$. This quantity then evolves slowly through viscous diffusion, the Reynolds number being equal to $\mathrm{Re}=\Gamma/\nu\approx 2750$. In Ref. 2, p. 91, the authors claim that the shortwave antisymmetric instability starts to be visible around $t=7s$, i.e., at $t\Gamma/2\pi b^2=4.9$, when the dipole aspect ratio is equal to $a/b=0.24$. According to Fig. 14 in the paper of Leweke and Williamson, this linear regime holds on at least until $t\Gamma/2\pi b^2=7.5$, where $a/b=0.285$. The observed eigenmode is antisymmetric and its wavenumber is found to be $kb=8.16$. The observed amplification rate is equal to $\sigma 2\pi b^2/\Gamma=0.94$.

These results have to be compared to those of the inviscid stability analyses achieved in Sec. III. For $a/b=0.208$ and $a/b=0.288$, maximum amplifications were obtained for $ka=2.26$, where $\sigma 2\pi b^2/\Gamma=1.38$. These discrepancies may be explained.

For the amplification rate, we have to account for the effect of viscosity on the perturbation. Landman and Saffman[7] showed that for a perturbation developing on an elliptical homogeneous flow this viscous correction term was $-4\nu k^2$. Hence, in the present case, the amplification rate when Re=2750 should read as $\sigma 2\pi b^2/\Gamma=1.38 -8\pi k^2 b^2/\mathrm{Re}=0.78$. This viscous correction seems too strong since the observed amplification rate is $\sigma 2\pi b^2/\Gamma =0.94$.

For the wavenumber, as suggested by Laporte and Corjon[25] and Laporte and Leweke,[26] one has to take into account the viscous diffusion of the basic flow. The core radius increases from $a/b=0.15$ at the beginning of the experiment up to $a/b=0.285$ at the end. Consequently, a perturbation such as $kb=8.16$ corresponds to $ka=1.60$ when $a/b=0.196$, $ka=2.26$ when $a/b=0.277$ and $ka=2.33$ when $a/b=0.285$. Hence, the stability analysis results seem to be recovered if the selection process is established when $a/b =0.277$. The above reasoning, which was suggested by Laporte and Corjon,[25] is erroneous since the instability starts to be visible when $a/b=0.24$, so that the perturbation grows for wavenumbers that satisfy $ka<8.16\times 0.24=1.96$. This result remains unexplained by the stability analysis which predicts $ka=2.26$.

In order to give a correct interpretation of the experiment of Leweke and Williamson, we now present a linear nonautonomous amplitude equation that takes into account the viscous effects that affect both the basic flowfield (an increase of the core radius a) and the amplification rate of the perturbation (the viscous correction of $\sigma 2\pi b^2/\Gamma$).

Note that this approach of an elliptic instability developing in a slowly diffusing Lamb–Oseen vortex has already been analyzed by Eloy and Le Dizès[12] for cases where $a/b \sim \lambda/\mathrm{Re}^{1/4}$ with $\mathrm{Re}\gg 1$, λ being a given constant. This scaling corresponds to vortices with high values of the aspect ratio a/b. In this case, the basic flow slowly evolves through viscous diffusion (a slowly increases), but the unstable eigenmode does not feel the viscosity. Indeed, using the viscous correction introduced by Landman and Saffman[7] and the above introduced scaling $a/b\sim\lambda/\mathrm{Re}^{1/4}$, the ratio between the viscous correction and the inviscid maximum amplification rate obtained for $ka=2.26$ reads as $4\nu k^2/[\Gamma/(2\pi b^2)] =8\pi(kb)^2/\mathrm{Re}\sim 8\pi(ka)^2/(\lambda^2\,\mathrm{Re}^{1/2})\sim 128/(\lambda^2\,\mathrm{Re}^{1/2})$ which is zero in the limit $\mathrm{Re}\gg 1$.

Now, the experiment of Leweke and Williamson, characterized by $a/b\sim 0.25$ and $\mathrm{Re}\sim 2750$, suggests the scaling $a/b\sim\chi/\mathrm{Re}^{1/2}$, χ being a given constant. This corresponds to lower values of the aspect ratio a/b. In this case, as observed in the experiment, the viscous evolution time scale of the dipole $T_\nu=2\pi a^2/\nu$ becomes equivalent to the instability time scale $T_\sigma=2\pi b^2/\Gamma$. Besides, viscosity now has an impact on the amplification rate of the perturbation since $4\nu k^2/[\Gamma/(2\pi b^2)] = 8\pi(kb)^2/\mathrm{Re}\sim 8\pi(ka)^2/\chi^2 \sim 128/\chi^2\sim \mathrm{cst}$ as $\mathrm{Re}\gg 1$.

B. A nonautonomous amplitude equation

1. Introduction

We consider the perturbation flowfield $e^{ikz}\mathbf{u}(x,y,t)$ with $\mathbf{u}=(u,v)^T$ where u and v stand for the x-component and y-component velocity perturbation. The z-component velocity perturbation w is related to u and v thanks to the incompressibility of the flowfield $\partial_x u+\partial_y v+ikw=0$.

We choose the following scalar product:[27] if $\mathbf{u}_1 =(u_1,v_1)^T$ and $\mathbf{u}_2=(u_2,v_2)^T$,

$$\langle \mathbf{u}_1,\mathbf{u}_2\rangle=\int_{-\infty}^{+\infty}\int_{-\infty}^{+\infty}(u_1^* u_2+v_1^* v_2)\,dx\,dy, \tag{12}$$

where the star denotes the complex conjugate. The norm of a perturbation is therefore related to the kinetik energy based on the x and y velocity components of the perturbation.

In the experiment of Leweke and Williamson, we have concentrated vortex dipoles with small values of a/b. Hence, in the following we assume that

$$\frac{da}{dt}=\frac{2\nu}{a}, \tag{13}$$

$$\frac{db}{dt}=0, \tag{14}$$

$$\frac{d\Gamma}{dt}=0. \tag{15}$$

Note that Eq. (13) characterizes the time evolution of a single Lamb–Oseen vortex but one can show[1,2] that this relation holds in vortex pairs when a/b remains small.

Choosing, $L=b$ and $T=2\pi b^2/\Gamma$ as length and time scales, the eigenmodes and eigenvalues depend on three parameters: a/b, kb and $\mathrm{Re}=\Gamma/\nu$. Remind that time dependance is achieved through the time evolution of the core radius a only.

In the following, $\mathbf{v}(a/b,kb,\Gamma/\nu)$ and $\mathbf{w}(a/b,kb,\Gamma/\nu)$ correspond to the unstable eigenmode and adjoint mode relative to the eigenvalue $[\sigma 2\pi b^2/\Gamma](a/b,kb,\Gamma/\nu)$. The eigenmode and the adjoint mode are normed in the following way: $\langle\mathbf{v},\mathbf{v}\rangle=1$ and $\langle\mathbf{w},\mathbf{v}\rangle=1$.

In Appendix A 3, we show that

$$\frac{d}{d\left(t\dfrac{\Gamma}{2\pi b^2}\right)}\left[\ln\frac{A}{A_0}\right]=\sigma\frac{2\pi b^2}{\Gamma}-\frac{4\pi}{\mathrm{Re}}\frac{b}{a}\left\langle \mathbf{w},\frac{\partial\mathbf{v}}{\partial(a/b)}\right\rangle, \tag{16}$$

where $A=\langle\mathbf{w},\mathbf{u}\rangle$ and A_0 is the initial amplitude of the eigenmode.

The first term on the rhs of this equation represents the amplification rate of a perturbation characterized by a wavenumber kb and a Reynolds number Re developing on a frozen basic flowfield with aspect ratio a/b. This term evolves in time because of the diffusion of the basic flowfield which results in an increase of a/b. This term also takes into account the effect of viscosity on the perturbation.

The second term on the rhs represents a correction term of the amplification rate due to the change in time of the unstable eigenmode shape which is due to the diffusion of

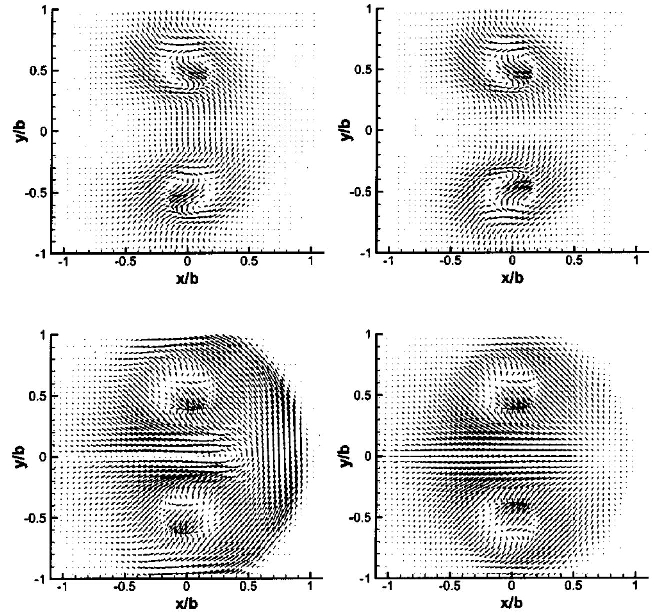

FIG. 8. Unstable eigenmodes and adjoint modes obtained for $kb=7.99$, $a/b=0.288$ and $\mathrm{Re}=2750$. Upper plots: eigenmodes, lower plots: adjoint modes. Left plots: antisymmetric modes, right plots: symmetric modes.

the basic flowfield. Indeed, the shape of the unstable eigenmode characterized by a fixed wavenumber kb changes slowly as a/b increases. Physically speaking, this correction term takes into account the re-projection at any time of the unstable eigenmode on the new unstable eigenmode. Note that a finite difference approach has been used to evaluate numerically the derivative $\partial \mathbf{v}/\partial(a/b)$. Note also that the adjoint mode $\mathbf{w}$ depends on the choice of the scalar product. But, the term $\langle \mathbf{w},\cdot\rangle$ is independent of that choice so that this correction term as well as relation (16) hold whatever the choice of the scalar product (12).

In the following sections, we numerically evaluate these two quantities as functions of a/b and kb for $\mathrm{Re}=2750$.

2. Eigenmodes, adjoint modes and eigenvalues

The spectral Chebyshev–Gauss collocation method presented in Sec. III is used to obtain the eigenvalues $[\sigma 2\pi b^2/\Gamma](a/b,kb,\Gamma/\nu)$, the eigenmodes $\mathbf{v}(a/b,kb,\Gamma/\nu)$ and the adjoint modes $\mathbf{w}(a/b,kb,\Gamma/\nu)$. An example of eigenmodes and adjoint modes is given in Fig. 8 for $kb=7.99$, $a/b=0.288$ and $\mathrm{Re}=2750$. The antisymmetric and symmetric eigenmodes (respectively, adjoint modes) are given on the two upper plots (respectively, lower plots). The antisymmetric and symmetric adjoint modes are quite different: the antisymmetric adjoint mode has a significant contribution on the right hyperbolic stagnation point whereas the symmetric adjoint mode has a significant contribution on the point situated at the middle of the two counter-rotating vortices. This proves that the receptivity of the antisymmetric and symmetric eigenmodes is different.

The norm of the adjoint mode versus kb is given in the upper plot of Fig. 9 for $\mathrm{Re}=2750$ and three values of the aspect ratio ($a/b=0.213,0.251,0.284$). The overall values around $\langle \mathbf{w},\mathbf{w}\rangle^{1/2}\approx 2$ are quite small, showing that non-normality is weak in the case of Widnall instabilities. Note,

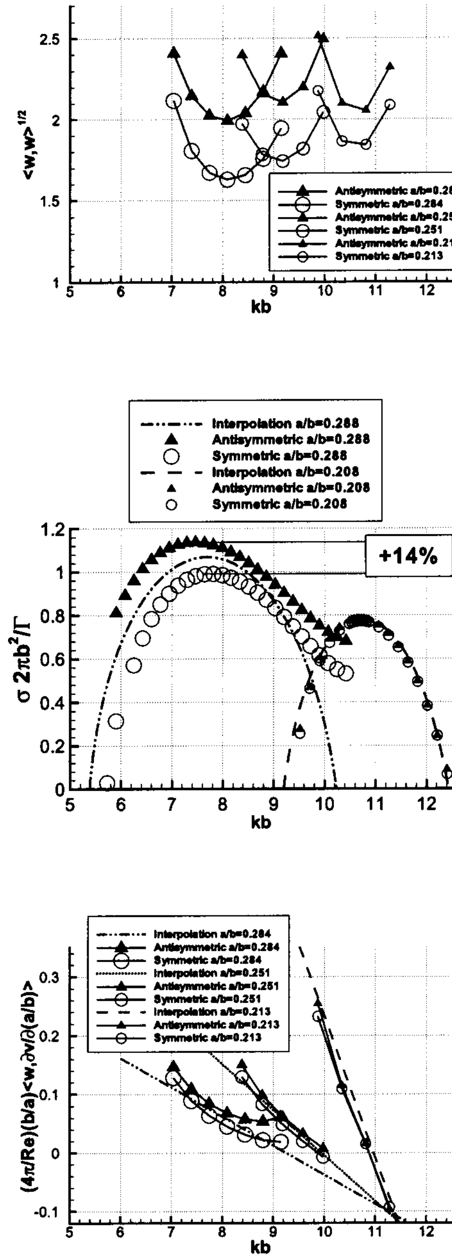

FIG. 9. Upper plot: Norm of adjoint mode versus kb. Middle plot: First term of the rhs of Eq. (16) versus kb. Lower plot: Second term of the rhs of Eq. (16) versus kb. Case: $\mathrm{Re}=2750$ and different values of aspect ratio a/b.

however, that the values of the antisymmetric eigenmodes are higher than those of the symmetric ones. This indicates that a non-normal behavior is more likely to appear in antisymmetric eigenmodes than in symmetric ones. For each aspect ratio a/b, the norm of the adjoint mode is smallest when the amplification rate is maximum. This can be seen when we compare the present plot to the middle plot of Fig. 9 showing the correponding unstable eigenvalues. Hence, non-normal features are more likely to appear when the unstable eigenvalues are small.

The middle and lower plots of Fig. 9 give the first and second term of the rhs of Eq. (16). In the middle plot of Fig. 9, it is shown that the amplification rates of the unstable antisymmetric eigenmodes are 14% larger than those of the symmetric ones in the case $a/b=0.288$. This value should be compared to the 7% obtained in the inviscid case. For $a/b = 0.208$, the antisymmetric and symmetric amplification rates are the same. It also appears that the viscous damping given by Landman and Saffman, obtained in the case of an instability developing in a homogeneous elliptical flow, is too strong here. As a matter of fact, Landman and Saffman give, for the viscous correction term, $\sigma 2\pi b^2/\Gamma = -8\pi k^2 b^2/\mathrm{Re}$ whereas the computations for the case $a/b = 0.208$ yield $\sigma 2\pi b^2/\Gamma = -4.5\pi k^2 b^2/\mathrm{Re}$ which is nearly two times smaller in amplitude.

In the lower plot of Fig. 9, we can see that the value of the correction term accounting for the slow evolution of the core radius a of the vortices is around 0.1. This value represents typically a loss of 10% of the initial value of the viscous amplification rate. Note also that for small values of a/b and high values of kb the correction term can be negative indicating a possible acceleration of the instability due to non-normality.

3. Interpolation of the different terms

In order to integrate numerically Eq. (16), we give analytical formulas which interpolate the results obtained in the middle and lower plots of Fig. 9. We do not distinguish here the antisymmetric and the symmetric eigenmodes.

The first and second terms of the rhs of Eq. (16) as functions of a/b and kb are interpolated in the following way:

$$\sigma \frac{2\pi b^2}{\Gamma} = \beta \sqrt{1 - \left[\frac{\alpha}{\beta}\left(kb\frac{a}{b} - 2.26\right)\frac{1}{(a/b)^2}\right]^2} - \frac{2\pi}{\mathrm{Re}}(kb)^2 - 6.3 \times \frac{2\pi}{\mathrm{Re}}\frac{1}{(a/b)^2}, \tag{17}$$

$$\frac{4\pi}{\mathrm{Re}}\frac{b}{a}\left\langle \mathbf{w}, \frac{\partial \mathbf{v}}{\partial(a/b)}\right\rangle = \frac{0.0046}{a/b}\left[4 - \left(kb - \frac{2.26}{a/b}\right) \times \left(2086\left(\frac{a}{b}\right)^2 - 1152\left(\frac{a}{b}\right) + 162\right)\right]. \tag{18}$$

Note that the viscous damping term acting on the amplification rate has been adjusted to fit the results for $a/b = 0.208$. These interpolations are valid roughly for $0.18 < a/b < 0.30$ and $\mathrm{Re} = 2750$. They are shown in the middle and lower plots of Fig. 9 in dashed, dotted and dashed–dotted lines. We see that the curves fit correctly the numerical results.

4. Results

We now integrate in time relation (16) in order to obtain the total growth of the pertubation as a function of time:

$$\ln \frac{A}{A_0} = \int \left[\sigma \frac{2\pi b^2}{\Gamma} - \frac{4\pi}{\mathrm{Re}}\frac{b}{a}\left\langle \mathbf{w}, \frac{\partial \mathbf{v}}{\partial(a/b)}\right\rangle\right] d\left(t\frac{\Gamma}{2\pi b^2}\right). \tag{19}$$

Be reminded that the interpolations are valid for $0.18 < a/b < 0.3$, i.e., $2.2 < t\Gamma/(2\pi b^2) < 8.5$ in the experiment.

In the upper plot of Fig. 10, we have sketched as a function of time the wavenumber k of the perturbation nondimensionalized by the core radius a. Three curves are displayed

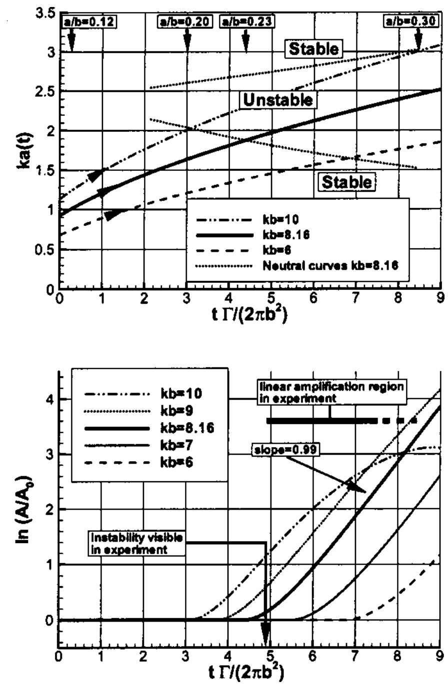

FIG. 10. Upper plot: Evolution of ka as a function of time for perturbations characterized by different values of kb. The dotted line corresponds to the neutral curve where the rhs of Eq. (16) is zero. Lower plot: Evolution of the growth of the perturbation as a function of time for different values of kb.

for three different values of kb. For each curve characterized by kb, ka increases as $(ka)(t) = kb \times a(t)/b$ where k, b are constants and $a(t)$ evolves following Eq. (13). The dotted lines represent, for $\mathrm{Re} = 2750$ and $kb = 8.16$, the neutral curves corresponding to the annulation of the rhs of Eq. (16), and which have been obtained from Eqs. (17) and (18). Note that the neutral curves obtained in the cases $kb = 6$ and $kb = 10$ are not displayed since they are nearly not distinguishable from the neutral curves obtained in the case $kb = 8.16$.

The amplitude of the perturbation grows when $ka(t)$ is located in the area enclosed by the two neutral curves and decays outside. Hence, at the beginning of the experiment $(t\Gamma/(2\pi b^2) = 0)$, perturbations are damped in all considered cases $(kb = 6, 8.16, 10)$. For $kb = 10$, the amplitude of the perturbation grows from time $t\Gamma/(2\pi b^2) = 3$ until $t\Gamma/(2\pi b^2) = 8.5$ where it starts decaying. The perturbation experiences a transient growth. The same behavior is observed for $kb = 8.16$ and $kb = 6$ but the perturbation amplitudes characterized, respectively, by $kb = 8.16$ and $kb = 6$ start growing later, i.e., at $t\Gamma/(2\pi b^2) = 4.2$ and $t\Gamma/(2\pi b^2) = 6.8$, respectively.

In the lower plot of Fig. 10, we have sketched versus time the growth of the perturbation amplitude. Several curves obtained for various wavenumbers ranging from $kb = 6$ to $kb = 10$ are shown. All these perturbations experience a transient growth: each perturbation characterized by a given value of kb appears at some time, grows exponentially with constant growth, then saturates before decaying again.

Following Leweke and Williamson, the observed perturbation in the experiment is characterized by $kb = 8.16$ and starts to be visible at $t\Gamma/(2\pi b^2) = 4.9$. The linear regime with constant growth rate equal to $\sigma 2\pi b^2/\Gamma = 0.94$ then holds on at least until $t\Gamma/(2\pi b^2)=7.5$. In our model, only the curves with $kb=8.16$ and $kb=9$ are compatible with these observations. Indeed, the perturbation obtained with $kb=10$ should appear earlier and the linear regime with constant growth rate should hold on only until $t\Gamma/(2\pi b^2)=6$. As well, the perturbations obtained for $kb=6$ and $kb=7$ should appear later, i.e., $t\Gamma/(2\pi b^2)>6$. The growth rate of the perturbation characterized by $kb=8.16$ is found to be $\sigma 2\pi b^2/\Gamma=0.99$, which has to be compared to the experimental value of $\sigma 2\pi b^2/\Gamma=0.94$. This prediction is quite good.

As a conclusion, this model shows that the experimentally observed wavenumber and growth rate of the perturbation are compatible with a model based on a linear nonautonomous amplitude equation that takes into account both the effect of viscosity on the perturbation and on the basic flow. It also helps understanding the selection of the antisymmetric eigenmode. Indeed, as mentioned earlier, the difference between the amplification rates of antisymmetric and symmetric eigenmodes reaches 14% for $kb=7.5$ in the case $a/b=0.288$ and $\mathrm{Re}=2750$.

VI. CONCLUSION

In the inviscid case, we have achieved a complete three-dimensional linear analysis of the Lamb–Oseen vortex for Kelvin waves characterized by $m=0$, $m=\pm 1$ and $m=\pm 2$. We have shown that the presence of critical layers damps a large number of co-rotating waves. As a consequence, only the stationary bending waves $(\omega=0, m=\pm 1, (ka)_c)$ may lead to Widnall instabilities. A weakly stretched Lamb–Oseen vortex is therefore not equivalent to a Rankine vortex, which displays additional oscillating Widnall instabilities resulting from the interaction of general m and $m+2$ Kelvin waves. We numerically calculated the amplification rates related to the resonances that occur for the stationary bending waves associated to the branches labeled 1, 2 and 3, following the asymptotic analysis of Moore and Saffman[4] and found the same results as Eloy and Le Dizès.[12] This asymptotic stability analysis is used as a reference problem for the normal mode analysis of the dipole family presented in Ref. 1, which are quasisteady solutions of the Euler equations. Two dipole aspect ratios have been considered. In the case $a/b=0.208$, the amplification rates of the symmetric and antisymmetric Widnall instabilities are very close. This means that the corresponding unstable eigenmodes may develop independently on each vortex. This result also shows that, in dipoles of aspect ratio equal to $a/b=0.2$, the linear regime is unable to promote the antisymmetric eigenmode. The amplification rates of the symmetric and antisymmetric eigenmodes collapse on the curves obtained by the asymptotic stability analysis of a weakly stretched Lamb–Oseen vortex. For higher dipole aspect ratios $a/b=0.288$, the amplification rates of the antisymmetric eigenmodes become 7% larger than those of the symmetric ones in the resonance region of the bending wave labeled 1.

In the viscous case, a linear nonautonomous amplitude equation for the development of a perturbation on a basic flowfield has been presented which takes into account both the effect of viscosity on the basic flowfield and on the perturbation. It was shown that this approach yields predictions for the amplification rate and for the wavenumber that agree with the experimental observations of Leweke and Williamson. Viscosity increases up to 14%, the difference between antisymmetric and symmetric eigenmode amplification rates in the case $a/b=0.288$ and $\mathrm{Re}=2750$. We have also shown that the receptivity of antisymmetric and symmetric eigenmodes is quite different: the antisymmetric adjoint mode has a significant contribution on one of the two hyperbolic stagnation points of the vortex pair whereas the symmetric adjoint mode has a significant contribution on the point situated at the middle of the two counter-rotating vortices. However, the small values of the norm of the adjoint modes show that non-normality is weak in the case of Widnall instabilities.

APPENDIX A: LINEAR DYNAMICS OF THE VORTEX PAIR

In this appendix we present the equations of the normal mode analysis for a plane basic flowfield and the numerical method which is used to solve these equations.

1. Normal mode approach

The Cartesian components of the velocity of the basic flow are

$$u=\psi_y, \quad v=-\psi_x, \quad w=0,$$

where $\psi(x,y)$ is the streamfunction and the subscripts x and y denote partial spatial derivatives. The normal modes are sought in the form $e^{\sigma t}e^{ikz}\phi(x,y)$ where $\phi=u',v',w',p'$ stands for the velocity and pressure perturbations. k is the real Oz wavenumber and σ is the complex amplification rate.

By linearizing the full incompressible Navier–Stokes equations around this basic flowfield, we obtain the following equations:

$$\left[(\sigma-\nu\Delta)\begin{pmatrix}0 & \Delta\\ \mathcal{V} & \mathcal{W}\end{pmatrix}-\begin{pmatrix}\mathcal{Q} & \mathcal{R}\\ \mathcal{S} & \mathcal{T}\end{pmatrix}\right]\begin{pmatrix}u'\\ v'\end{pmatrix}=0, \tag{A1}$$

with the following linear operators:

$$\Delta=\partial_{xx}+\partial_{yy}-k^2, \tag{A2}$$

$$\mathcal{V}=\partial_{xx}-k^2, \tag{A3}$$

$$\mathcal{W}=\partial_{xy}, \tag{A4}$$

$$\mathcal{Q}=\psi_{xx}(\partial_{xx}-\partial_{yy}-k^2)+2\psi_{xy}\partial_{xy}-2W_x\partial_x-W_{xx}, \tag{A5}$$

$$\mathcal{R}=-(\psi_y\partial_x-\psi_x\partial_y-\psi_{xy})\Delta-2\psi_{xy}\partial_{xx}+2\psi_{xx}\partial_{xy} -W_x\partial_y-W_y\partial_x-W_{xy}, \tag{A6}$$

$$\mathcal{S}=-(\psi_y\partial_x-\psi_x\partial_y+\psi_{xy})(\partial_{xx}-k^2)+\psi_{xx}\partial_{xy}, \tag{A7}$$

$$\mathcal{T}=-(\psi_y\partial_x-\psi_x\partial_y+\psi_{xy})\partial_{xy}+\psi_{xx}(\partial_{yy}+k^2)-k^2W. \tag{A8}$$

In these expressions, $\partial_{xy}=\partial^2/\partial x\partial y$, etc., and W is the Oz vorticity of the basic flowfield: $W=-(\psi_{xx}+\psi_{yy})$. ν is the kinematic viscosity.

2. Spectral Chebyshev–Gauss collocation method

We use a spectral Chebyshev–Gauss collocation method to discretize the remaining x and y derivatives (see Ref. 28).

First, we map the infinite domain $-\infty<x,y<\infty$ on $-1<\xi_x,\xi_y<1$:

$$x=f(\xi_x),\ \text{where}\ |\xi_x|<1\ \text{and}\ |x|<\infty;$$
$$y=g(\xi_y),\ \text{where}\ |\xi_y|<1\ \text{and}\ |y|<\infty; \tag{A9}$$

$$f(\xi_x)=H_x\tanh^{-1}\xi_x+\Lambda_x\,\mathrm{erf}(\xi_x/\Upsilon_x); \tag{A10}$$

$$g(\xi_y)=H_y\tanh^{-1}\xi_y+\Lambda_y\,\mathrm{erf}(\xi_y/\Upsilon_y). \tag{A11}$$

H_x, H_y, Λ_x, Λ_y, Υ_x and Υ_y are constants and erf is the standard error function.

We use the exponential mapping in (A9) because eigenmodes decrease exponentially at large distances. An additional term, built with the standard error function, has been introduced for better localization of the collocation points on the vortices. The contribution of this term vanishes at large distances so that the asymptotic properties of the $\tanh^{-1}$ function is preserved.

The unknowns $\phi=u',v'$ are then expanded in a double truncated Chebyshev series:

$$\phi(x,y)=\sum_{i=0}^{N_x}\sum_{j=0}^{N_y}\hat{\phi}_{i,j}T_i(\xi_x)T_j(\xi_y), \tag{A12}$$

with N_x+1 and N_y+1 Chebyshev polynomials $T_n(\xi)$ in each direction.

The unknowns $\hat{\phi}_{i,j}=\hat{u}'_{i,j},\hat{v}'_{i,j}$ are then determined by enforcing Eqs. (A1) at $(N_x+1)(N_y+1)$ points in the square $-1<\xi_x,\xi_y<1$. This method is particularly efficient if we take the Chebyshev–Gauss points:

$$\xi_i=\cos\left(\frac{2i+1}{2N_x+2}\pi\right),\quad i=0\cdots N_x\quad\text{and}$$
$$\xi_j=\cos\left(\frac{2j+1}{2N_y+2}\pi\right),\quad j=0\cdots N_y.$$

Calculations are performed in physical space so that the unknowns are the values of $(u'(\xi_i,\xi_j),v'(\xi_i,\xi_j))$ at each node of the grid in physical space. We are thus led to a generalized eigenvalue problem of the form $B\mathbf{v}=\sigma C\mathbf{v}$ where B and C are two matrices, σ is the complex eigenvalue and $\mathbf{v}$ is the eigenvector which contains the values of u' and v' at all nodes. Eigenvalues and eigenvectors are determined by a standard QR method.

3. A nonautonomous amplitude equation

We now consider a basic flowfield that evolves with time, so that from now on the matrix B depends on time. The perturbation flowfield $e^{ikz}\mathbf{u}(x,y,t)$ with $\mathbf{u}=(u,v)^T$ is governed by the following equation:

$$\frac{\partial\mathbf{u}(t)}{\partial t}=D(t)\mathbf{u}(t), \tag{A13}$$

where $D(t)=C^{-1}B(t)$.

If $\mathbf{u}_1=(u_1,v_1)^T$ and $\mathbf{u}_2=(u_2,v_2)^T$, the scalar product introduced in (12) reads as

$$\langle\mathbf{u}_1,\mathbf{u}_2\rangle=\frac{\pi^2}{(N_x+1)(N_y+1)}\sum_{i=0}^{N_x}\sum_{j=0}^{N_y}[u_1^*(\xi_i,\xi_j)u_2(\xi_i,\xi_j)+v_1^*(\xi_i,\xi_j)v_2(\xi_i,\xi_j)]f'(\xi_i)g'(\xi_j), \tag{A14}$$

$$=\mathbf{u}_1^{\mathrm{H}}N\mathbf{u}_2, \tag{A15}$$

where N is a positive definite diagonal matrix, so that $N^{\mathrm{H}}=N$. Here the superscript H designates the Hermitian.

We therefore consider the following generalized eigenvalue problem:

$$M(t)\mathbf{v}=\sigma N\mathbf{v}, \tag{A16}$$

where $M(t)=ND(t)$ with $M^{\mathrm{H}}=M^T$. Here $\mathbf{v}$ is an eigenvector associated to the eigenvalue σ.

The eigenmodes $\mathbf{v}_i(t)$, adjoint modes $\mathbf{w}_i(t)$ and eigenvalues $\sigma_i(t)$ of this generalized eigenvalue problem, parametrized by time, verify

$$M(t)\mathbf{v}_i(t)=\sigma_i(t)N\mathbf{v}_i(t), \tag{A17}$$

$$M^T(t)\mathbf{w}_i(t)=\sigma_i^*(t)N\mathbf{w}_i(t), \tag{A18}$$

$$\mathbf{v}_i^{\mathrm{H}}(t)N\mathbf{v}_i(t)=1, \tag{A19}$$

$$\mathbf{w}_i^{\mathrm{H}}(t)N\mathbf{v}_i(t)=1. \tag{A20}$$

At any time, $\mathbf{u}(t)$ can be expressed in the basis formed by the eigenvectors $\mathbf{v}_i(t)$ following

$$\mathbf{u}(t)=\sum_i[\mathbf{w}_i^{\mathrm{H}}(t)N\mathbf{u}(t)]\mathbf{v}_i(t). \tag{A21}$$

We now consider one particular eigenvector $\mathbf{v}(t)$, adjoint mode $\mathbf{w}(t)$ and eigenvalue $\sigma(t)$. We are interested in the time evolution of $A(t)=\mathbf{w}^{\mathrm{H}}(t)N\mathbf{u}(t)$, which corresponds to the projection of the perturbation field $\mathbf{u}(t)$ on the eigenvector $\mathbf{v}(t)$.

Equation (A13) yields the following relation: $\mathbf{w}^{\mathrm{H}}(t)N(\partial\mathbf{u}(t)/\partial t)=\mathbf{w}^{\mathrm{H}}(t)M(t)\mathbf{u}(t)$ so that

$$\frac{d}{dt}[\mathbf{w}^{\mathrm{H}}(t)N\mathbf{u}(t)]=[M^T(t)\mathbf{w}(t)]^{\mathrm{H}}\mathbf{u}(t)+\left[\frac{\partial\mathbf{w}(t)}{\partial t}\right]^{\mathrm{H}}N\mathbf{u}(t), \tag{A22}$$

$$=[\sigma^*(t)N\mathbf{w}(t)]^{\mathrm{H}}\mathbf{u}(t)+\left[\frac{\partial\mathbf{w}(t)}{\partial t}\right]^{\mathrm{H}}N\sum_i\mathbf{v}_i(t)[\mathbf{w}_i^{\mathrm{H}}(t)N\mathbf{u}(t)], \tag{A23}$$

$$=\sigma(t)[\mathbf{w}^{\mathrm{H}}(t)N\mathbf{u}(t)]+\sum_i\left[\left[\frac{\partial\mathbf{w}(t)}{\partial t}\right]^{\mathrm{H}}N\mathbf{v}_i(t)\right][\mathbf{w}_i^{\mathrm{H}}(t)N\mathbf{u}(t)], \tag{A24}$$

$$\approx\sigma(t)[\mathbf{w}^{\mathrm{H}}(t)N\mathbf{u}(t)]+\left[\left[\frac{\partial\mathbf{w}(t)}{\partial t}\right]^{\mathrm{H}}N\mathbf{v}(t)\right][\mathbf{w}^{\mathrm{H}}(t)N\mathbf{u}(t)]. \tag{A25}$$

TABLE I. Bending modes: a comparison between values given by the shooting method (second column) and values given by the 2-D collocation method (third column). Only significant digits have been retained.

Mode label	Shooting method	2-D collocation method
0	0.52769697	0.52769697
1	0.057086548	0.0570865
$0'$	-1.6340331	-1.634033
$1'$	-1.4052029	-1.40520
$2'$	-1.2852558	-1.28
$3'$	-1.2135359	??

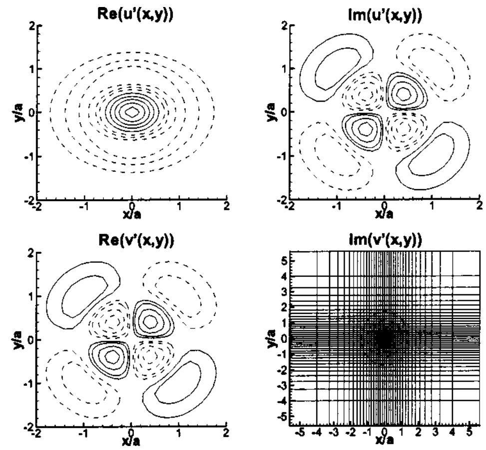

FIG. 11. One Lamb–Oseen vortex: eigenfunction of the bending mode labeled 1 in the case $ka=2.6764054$. Dashed lines represent negative isovalues. The location of the collocation points is given for $\mathrm{Im}(v'(x,y))$. Re( ) and Im( ) here designate real and imaginary parts of a complex.

In order to obtain this last result, we have assumed that, at any time, nearly all the energy of the perturbation $e^{ikz}\mathbf{u}(x,y,t)$ is in the unstable eigenmode $\mathbf{v}$. This is likely to be the case in the experiment of Leweke and Williamson[2] where only one identified smooth perturbation emerges from the basic flow at some given wavelength.

One can then easily deduce that

$$\frac{d}{dt}\left(\ln\frac{A}{A_0}\right)=\sigma(t)-\mathbf{w}^{\mathrm{H}}(t)N\frac{\partial\mathbf{v}(t)}{\partial t},\tag{A26}$$

where $A(t)=\mathbf{w}^{\mathrm{H}}(t)N\mathbf{u}(t)$ and $A_0=A(t=0)$.

The basic flowfield which evolves in time is characterized at any time by the dipole aspect ratio a/b. The eigenmode, the adjoint mode and the eigenvalue therefore depend on a/b. They also depend on the spatial structure of the perturbation in the z direction which is given by the nondimensional wavenumber kb and the level of viscosity acting on the perturbation and which is measured here by the Reynolds number $\mathrm{Re}=\Gamma/\nu$. Hence, we note $[\sigma 2\pi b^2/\Gamma](a/b,kb,\Gamma/\nu)$, $\mathbf{v}(a/b,kb,\Gamma/\nu)$ and $\mathbf{w}(a/b,kb,\Gamma/\nu)$. The dependence on time is then recovered using Eqs. (13), (14) and (15). It is then easy to show that

$$\frac{\partial\mathbf{v}(t)}{\partial t}=\frac{1}{b}\frac{da}{dt}\frac{\partial\mathbf{v}}{\partial(a/b)}=\frac{\Gamma}{2\pi b^2}\frac{4\pi}{\mathrm{Re}}\frac{b}{a}\frac{\partial\mathbf{v}}{\partial(a/b)}.\tag{A27}$$

With Eq. (A26), we obtain the following final result:

$$\frac{d}{d\left(t\frac{\Gamma}{2\pi b^2}\right)}\left[\ln\frac{A}{A_0}\right]=\sigma\frac{2\pi b^2}{\Gamma}-\frac{4\pi}{\mathrm{Re}}\frac{b}{a}\left[\mathbf{w}^{\mathrm{H}}N\frac{\partial\mathbf{v}}{\partial(a/b)}\right].\tag{A28}$$

4. Comparisons between the shooting method and the spectral Chebyshev–Gauss collocation method for a single Lamb–Oseen vortex

The eigenvalues/eigenvectors given by the spectral Gauss collocation method are compared here to the shooting method in the case of a single Lamb–Oseen vortex.

The computation has been performed with the following parameters: $ka=2.6764054$, $\mathrm{Re}=\infty$. We use 36 Chebyshev polynomials in the x and y directions and the exponential mapping was chosen with $H_x=H_y=1.4548$, $\Upsilon_x=\Upsilon_y=1$, $\Lambda_x=\Lambda_y=0$. Comparisons between eigenvalues obtained with this code and eigenvalues given by the shooting method are listed in Table I for bending modes. Only significant digits have been given and the question mark means that the spatial resolution is not sufficient to capture the corresponding eigenfunction. Agreement is excellent for eigenmodes which have a simple spatial structure. For example, the bending mode labeled $0'$, with no zero in the radial direction, is obtained with a precision of seven digits whereas the mode labeled $2'$, with two zeros in the radial direction, is determined with a precision of only three digits.

Examples of eigenvectors are given in Fig. 11. The radial and azimuthal structure of the eigenmodes enable us to build a strict relation with the eigenmodes given by the shooting method.

As explained in Sec. IV B 2, bending waves whose frequencies lie in the range $-1<\omega_r 2\pi a^2/\Gamma<0$ exhibit critical layers. Therefore, integration should cope with the complex plane in order to capture these Kelvin waves. But this is not the case here and our code can therefore not extract these modes. Nevertheless when the corresponding critical layer is located at large distances from the vortex center (compared to the core radius), the viscous layer has little influence on the spatial structure of the normal mode and our code is able to extract it. This is what happened with the present calculation since eigenmodes corresponding to the bending waves 2 and 3 have been obtained. These modes are purely oscillatory and the frequencies $\omega 2\pi a^2/\Gamma$ are, respectively, 0.1094 and 0.1437. These values have to be compared with those given by the shooting method which are complex values: $0.109504+0.0001441i$ and $0.1467+0.0002684i$. The corresponding critical layers are located at $r_c/a=3.3870+0.002231i$ and $r_c/a=2.8894+0.2639i$. We can notice a deterioration of the precision as the critical point penetrates in the vortex.

5. Computations with the vortex pairs

The normal mode analyses of the vortex pairs are done using the following parameter settings. In the case of inviscid calculations, we use 34 Chebyshev polynomials in the x direction and 70 in the y direction. The exponential mapping was chosen with $H_x=0.3134$, $\Upsilon_x=0$, $\Lambda_x=1$, $H_y=0.3106$,

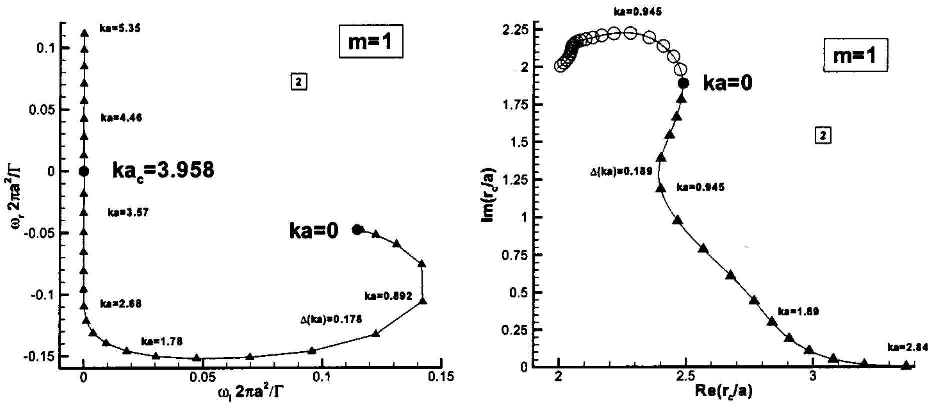

FIG. 12. Bending wave labeled 2 in the $m=1$ case: evolution of the eigenfrequency $\omega 2\pi a^2/\Gamma$ in the complex ω plane (left) and of the corresponding critical point r_c in the complex r plane (right), for ka varying from 5.35 to 0.

$\Upsilon_y=0.2937$ and $\Lambda_y=1.5620$. In the case of viscous calculations, we use 70 Chebyshev polynomials in the x and y directions. The exponential mapping was chosen with $H_x=0.50$, $\Upsilon_x=0.45$, $\Lambda_x=1.50$, $H_y=0.65$, $\Upsilon_y=0.2937$ and $\Lambda_y=1.5620$.

APPENDIX B: CRITICAL LAYERS

In this appendix, we discuss briefly the critical layers in the Kelvin waves. We focus on the Kelvin wave labeled 2 in the $m=1$ case (see Fig. 6). In the left plot of Fig. 12, we gave the locus of the eigenvalues $\omega 2\pi a^2/\Gamma$ in the complex ω plane, for ka varying from 5.35 to 0. We see that the eigenmodes are purely oscillatory if $ka>3.958$. When the wavenumber ka further diminishes, the frequency ω becomes complex with a positive imaginary part, which means that the mode is damped. In the right plot of Fig. 12, we have sketched the locus of the corresponding critical points r_c, defined as $\gamma(r_c)=0$, for ka varying from 3.958 to 0. Now, $r_c(\omega)$ involves the classical Lambert function which is a multi-valued complex function. Therefore, there exists an infinite number of critical points. The filled triangles represent the principal (or zero) branch whereas the empty circles represent the first branch. Following Refs. 18 and 29, the integration path has to lie above the critical point defined by the zero branch in order to select the valid eigenvalue/eigenvector when introducing viscosity. It also has to pass below the critical point defined by the first branch. As the wavenumber ka decreases, the viscous sector on the real axis penetrates into the vortex. This viscous sector is approximately centered at the real part of r_c and is located at infinity when $ka=3.958$. Finally, when $ka\rightarrow 0$ we have the following behavior: $\omega 2\pi a^2/\Gamma \rightarrow -0.0474+0.1144i$ and $r_c/a \rightarrow 2.51+1.88i$ which corresponds to the point where the critical point given by the zero and the first branch coincide. This property is valid for all branches.

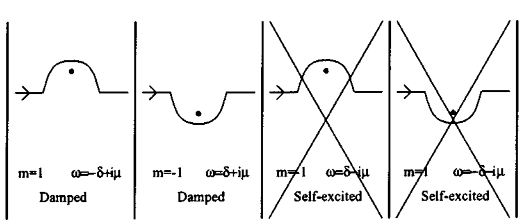

FIG. 13. A typical configuration for a damped bending wave: the four plots represent the integration path and position of the critical point r_c for the different eigenvalues (ω,m), $(-\omega^*,-m)$, $(-\omega,-m)$ and (ω^*,m). The two modes which have to be removed when introducing viscosity are scored out.

The eigenvalue problem (7) exhibits the following symmetries: if (ω,m) is an eigenvalue, then $(-\omega,-m)$, (ω^*,m) and $(-\omega^*,-m)$ are also eigenvalues. Now, when we consider the inviscid case as an asymptotic limit of the viscous case when $\nu\rightarrow 0$, two out of four solutions have to be removed and only the symmetry ω and $-\omega^*$ remains. In Fig. 13, we have sketched the critical point and the integration path of a typical quadruplet of solutions $\omega=\pm\delta\pm i\mu$ where $\delta>0$ and $\mu>0$. The two eigenvalues that must be removed are scored out in accordance with Ref. 18.

[1]D. Sipp, L. Jacquin, and C. Cossu, ‘‘Self-adaptation and viscous selection in concentrated two-dimensional vortex dipoles,’’ Phys. Fluids **12**, 245 (2000).
[2]T. Leweke and C. H. K. Williamson, ‘‘Cooperative elliptic instability of a vortex pair,’’ J. Fluid Mech. **360**, 85 (1998).
[3]S. C. Crow, ‘‘Stability theory of a pair of trailing vortices,’’ AIAA J. **8**, 2172 (1970).
[4]D. W. Moore and P. G. Saffman, ‘‘The instability of a straight vortex filament in a strain field,’’ Proc. R. Soc. London, Ser. A **346**, 413 (1975).
[5]C.-Y. Tsai and S. E. Widnall, ‘‘The stability of short waves on a straight vortex filament in a weak externally imposed strain field,’’ J. Fluid Mech. **73**, 721 (1976).
[6]S. E. Widnall, D. B. Bliss, and C.-Y. Tsai, ‘‘The instability of short waves on a vortex ring,’’ J. Fluid Mech. **66**, 35 (1974).
[7]M. J. Landman and P. G. Saffman, ‘‘The three-dimensional instability of strained vortices in a viscous fluid,’’ Phys. Fluids **30**, 2339 (1987).
[8]P. Billant, P. Brancher, and J.-M. Chomaz, ‘‘Three-dimensional stability of a vortex pair,’’ Phys. Fluids **11**, 2069 (1999).
[9]H. Lamb, *Hydrodynamics* (Cambridge University Press, Cambridge, 1906).
[10]V. V. Meleshko and G. J. F. van Heijst, ‘‘On Chaplygin's investigations of two-dimensional vortex structures in an inviscid fluid,’’ J. Fluid Mech. **272**, 157 (1994).
[11]D. Sipp, ‘‘Weakly nonlinear saturation of short-wave instabilities in a strained Lamb–Oseen vortex,’’ Phys. Fluids **12**, 1715 (2000).
[12]C. Eloy and S. Le Dizès, ‘‘Three-dimensional instability of Burgers and Lamb–Oseen vortices in a strain field,’’ J. Fluid Mech. **378**, 145 (1999).
[13]R. T. Pierrehumbert, ‘‘Universal short-wave instability of two-dimensional eddies in an inviscid fluid,’’ Phys. Rev. Lett. **57**, 2157 (1986).
[14]B. J. Bayly, ‘‘Three-dimensional instability of elliptical flow,’’ Phys. Rev. Lett. **57**, 2160 (1986).
[15]F. Waleffe, ‘‘On the three-dimensional instability of strained vortices,’’ Phys. Fluids A **2**, 76 (1990).
[16]L. N. Howard and A. S. Gupta, ‘‘On the hydrodynamic and hydromagnetic stability of swirling flows,’’ J. Fluid Mech. **14**, 463 (1962).

[17]M. Lessen, P. J. Singh, and F. Paillet, ''The stability of a trailing line vortex. Part 1. Inviscid theory,'' J. Fluid Mech. **63**, 753 (1974).
[18]C. C. Lin, *The Theory of Hydrodynamic Stability* (Cambridge University Press, Cambridge, 1955).
[19]P. G. Saffman, *Vortex Dynamics* (Cambridge University Press, Cambridge, 1992).
[20]S. E. Widnall, D. Bliss, and A. Zalay, ''Theoretical and experimental study of the stability of a vortex pair,'' In *Aircraft Wake Turbulence and Its Detection*, edited by J. H. Olsen, A. Goldburg, and M. Rogers (Plenum, New York, 1971), pp. 305–338.
[21]S. Leibovich, S. N. Brown, and Y. Patel, ''Bending waves on inviscid columnar vortices,'' J. Fluid Mech. **173**, 595 (1986).
[22]D. J. Benney and R. F. Bergeron, Jr., ''A new class of nonlinear waves in parallel flows,'' Stud. Appl. Math. **48**, 181 (1969).
[23]D. J. Benney and S. A. Maslowe, ''The evolution in space and time of nonlinear waves in parallel shear flows,'' Stud. Appl. Math. **LIV**, 181 (1975).
[24]S. le Dizès, ''Non-axisymmetric vortices,'' J. Fluid Mech. **406**, 175 (2000).
[25]F. Laporte and A. Corjon, ''Direct numerical simulations of the elliptic instability of a vortex pair,'' Phys. Fluids **12**, 1016 (2000).
[26]F. Laporte and T. Leweke, ''Elliptic instability of counter-rotating vortices: Experiment and direct numerical simulation,'' AIAA J. **40**, 2483 (2002).
[27]P. J. Schmid and D. S. Henningson, *Stability and Transition in Shear Flows* (Springer-Verlag, Berlin, 2001).
[28]C. Canuto, M. Y. Hussaini, A. Quateroni, and T. A. Zang, *Spectral Methods in Fluid Dynamics* (Springer-Verlag, Berlin, 1988).
[29]W. Wasow, *Asymptotic Expansions for Ordinary Differential Equations* (Interscience, New York, 1965).